VOL. 18, NO. 2, JANUARY 2023 ISSN 1819-6608
ARPN Journal of Engineering and Applied Sciences


www.arpnjournals.com

# MULTI-CLASS CLASSIFICATION OF PROSTATE CANCER MR IMAGES BASED ON UCLA SCORE USING REGNETY320 MODEL

Rajesh M. N. and Chandrasekar B. S
Department of Electronics and Communication Engineering, Faculty of Engineering and Technology, Jain, Bangalore, Karnataka, India
E-Mail: rajeshmn.mn@gmail.com

**ABSTRACT**

Prostate cancer (PCa) is the most frequent non-skin cancer in males, and it represents a significant global health care problem. Another challenge is the development of an accurate classification model for the detection of PCa. As a result, developing an accurate classification model for PCa is extremely important and has potentially significant clinical implications. These models have the potential to boost the benefits of treatment while also increasing the likelihood of a patient's survival. The PCa is classified in this research based on the T2w magnetic resonance images (MRI), which are collected from prostate dataset. In this work, a deep learning-based approach RegNetY-320 model is proposed to classify and detect the PCa. The RegNet model is a pretrained deep transfer learning architecture, which is most commonly used for the image classification process. The proposed model is optimized using various optimizers, including Adam, AdaMax, SGD, RMSprop, Ftrl, and Nadam, and the optimized models are termed as model-01 to model-06. For the evaluation, a multiclass classification system was employed to classify 845 patient records from an mpMRI dataset with a unique "UCLA" score of the ROI. Accuracy, precision, sensitivity, specificity, and the F1 score are all calculated based on the classification for the purpose of performance analysis. Finally, in accordance with the findings, the performances of the various proposed models are evaluated in order to determine their validity. When compared among proposed models, the proposed model RegNetY-320_Model-03 optimized using the RMSprop optimizer has obtained greater performance with 95.70 percent accuracy, which is the highest accuracy performance obtained in this research.

**Keywords:** PCa classification, optimizers, RegNetY, MRI, T2w, deep learning.

## 1. INTRODUCTION

Globally, PCa is the third most frequent disease and second most cancer commonly occurred in males, according to the World Health Organization. According to estimates, there was 1.4 million new PCa cases and 375,000 new PCa deaths worldwide in 2020 [1]. As a result, accurate and timely identification of PCa is critical in order to obtain effective overall patient outcomes. Digital rectal examination, PSA screening, transrectal ultrasound, and MRI are some of the methods available for examining and diagnosing PCa. In this regard, the MRI has attracted the greatest amount of attention over the past decade due to its efficient accuracy [2].

Recent technical advancements in the field of MRI have showed greater vision of the prostate when compared to ultrasound, and have also demonstrated the potential to detect malignant tumors in the prostate. In part, this is because transrectal ultrasound-guided biopsy is still remained as a "blind" approach of sampling since it was impossible to specify suspicious lesions precisely inside the prostate glands, particularly among PSA-positive cancer where disease was non-palpable because of their iso-echoic type, which means they are "invisible." To address this problem, systematic sampling must be implemented to increase the likelihoods of finding cancers. Although, this remains a flawed diagnostic, with a high number of tumors being unidentified by the procedure [3].

MRI in prostate has evolved into a significant technique in the diagnosis of PCa. The interpretation of prostate MRI was generally acknowledged to have a high learning progression. Deep learning, enabled by artificial intelligence, may enable more constant interpretations across radiologists with varying degrees of experiences, enhancing inter-reader agreements, and minimizing the requirement for specialized training in MRI interpretations for PCa [4].

**Table-1.** PCa scoring on T2w-MR images based on PI-RADS [5].

| Score | T2W | Description |
|---|---|---|
| 1 | 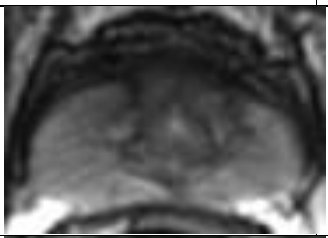 | Homogeneous intermediate signal intensity (normal). |
| 2 | 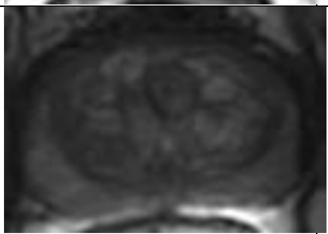 | Circumscribed hypointense or heterogeneous encapsulated nodule(s) (BPH). |
| 3 | 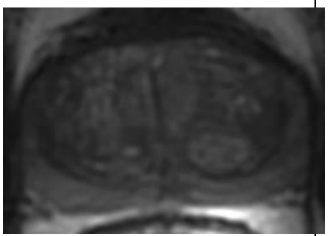 | Heterogeneous signal intensity with obscured margins. Includes those not qualifying for 1, 2, 4 or 5. |
| 4 | 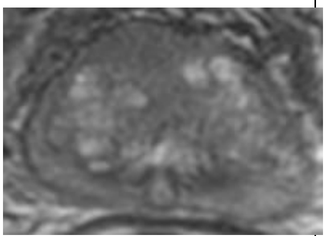 | Lenticular or non-circumscribed, homogeneous, moderately hypointense, and <1.5 cm in greatest dimension. |
| 5 | 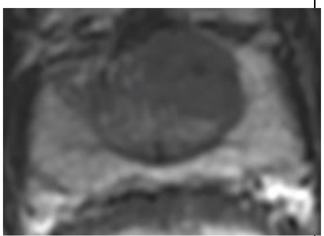 | Same as 4, but ≥1.5 cm in greatest dimension or definite extra prostatic extension/ invasive behavior. |

The use of imaging technology can help to mitigate the problem of sampling error to some extent. Combining MRI with ultrasound-guided biopsies can make it easier to collect samples from the most suspicious areas. Multiparametric magnetic resonance imaging (mpMRI) has evolved this strategy; the MRI-targeted biopsy was less possibly to miss higher grade PCa and reduces the prevalence of repeated biopsies when used in conjunction with other imaging techniques. When the pre-test chance of PCa being present is minimal, the European Association of Urology clearly recommends that imaging modalities, like multiparametric MRI, be investigated before to proceeding with biopsy, according to their clinical recommendations. Prostate exams have been standardized throughout the world, and the PI-RADS (Prostate Imaging Reporting and Data System) has been developed to ensure that all reports are consistent. mpMRI was a sort of non-invasive imaging that combines conventional anatomical sequences such as T2weighted images (T2W) and perfusion imaging, such as diffusion-weighted images (DWI) with apparent diffusion coefficient maps (ADC) and T1-weighted images (T1W), to generate dynamic contrast-enhanced images (DCE) [6-8].

In this research, a RegNetY-320 model with a pretrained deep transfer learning architecture was presented for the classification of PCa using T2w-MR images. Because of the remarkable classification accuracy of pretrained models, the transfer learning technique was selected as the preferred classification model in this work above other machine learning algorithms. Additionally, pretrained models save time consumption by ignoring the problem of retraining and testing the approach weights from the scratch.

To conduct this analysis, a pretrained deep transfer learning architecture RegNetY-320 model was proposed to classify PCa using T2w-MR images. Several convolutional and fully linked layers at the top of this network helped to the fine-tuning of the overall architecture. It is observed that a significant portion of the transfer learning approach relies on features extracted from the last convolutional layer and classification performed by the last fully connected layers, both of which are not generalizable to every dataset, as demonstrated by multiple experiments on the acquired dataset. Therefore, only these layers were considered for weight-training purposes. This strategy not only lowered the amount of time required, but it also increased the accuracy of the results. A number of different optimizers with appropriate learning rates are used to optimize the RegNetY-320 model as well. The proposed model was trained and tested using the PCa dataset, which was based on these optimizers with learning rates.

## 2. REVIEW OF RELATED WORKS

mpMRI is an accurate imaging modality for the identification of PCa; moreover, it required the skill of experienced specialists, resulting in inconsistent results across readers with varied levels of competence. In [9], a deep convolutional neural network (CNN) architecture was proposed for PCa detection on mpMRI in order to discover a more effective solution. This model was capable of learning lesion differentiating features from the mpMR images that were provided to it. A shortcoming of this model was the loss of information that occurred during image compression in order to meet the requirements of employing CNN architectures to compress images. Despite the fact that the implementation of the histogram approach was employed to transform the medical images, there was some information loss in the model.

According to [10], an automated PCa detection system based on deep CNN features and the single-stage

VOL. 18, NO. 2, JANUARY 2023 ISSN 1819-6608
ARPN Journal of Engineering and Applied Sciences



SVM approach could simultaneously detect the existence of PCa in the images and pinpoint lesion in the image. To be more specific, the co-trained CNNs that have been constructed were composed of two parallel convolution networks for T2w and ADC images, individually. Using images from the single model and in a weakly-supervised way, each network was trained by supplying a collection of PCa images with labels of image-level representing just the existence of PCa and no prior information about the location of lesions on the prostate. The CNN features of all the modalities were concatenated and input into an SVM approach, which was trained on the concatenated features. Adaptive thresholding and non-maximum suppression were used for the corresponding PCa response maps for the purpose of determining the location of PCa foci in images that were classified as containing malignancies. Thus, this work just addressed the creation of co-trained CNNs for integrating T2w and ADC images, it should have been expanded to include other imaging modalities, and multimodal fusion approaches might have been implemented.

FocalNet, a multi-class CNN, was introduced in [11] for jointly identifyingPCa lesion and forecast its aggressiveness with the Gleason scores, and it has been used to successfully do so. Specifically, an ordinal encoding was developed in FocalNet to quantify aggressiveness of lesions and loss of mutual finding in order to completely use knowledge in mpMR imaging. Non-experts can benefit from this FocalNet model, which claims to be able to support less experienced specialists and to enhance the PCaidentification process for them. Although the performance of this model was not great, where its sensitivity and specificity were both only 89.7 percent and 87.9 percent and there was one false positive/patient. It also obtained sensitivity and specificity that were only 3.4 percent and 1.5 percent minimum than experienced specialists using PI-RADS v2.

In [12], a hierarchical classification approach was developed for the identification of PCa. The concept of this work was to extract the high-level feature representation for PCa detection by employing deep neural networks, and then to create a hierarchical classification model based on the high-level feature representation. PCa detection findings were refined by the use of multiple random forest classifiers that were developed iteratively. This technology directly identifies cancer locations in the prostate mpMR images without the need for any additional imaging.

Using a multi-classification task for PCa detection, an end-to-end framework (PCa-GGNet-v2) was proposed in [13]. This process combined deep CNN and deep reinforcement learning for Gleason grade groups-radical prostatectomy of the patient-level, which was a multi-classification task for detecting PCa. With the PCa-GGNet-v2, radiologists could learn from each other to produce slice-level discoveries that could be used to make patient-level decisions. This allowed for collaborative optimization while avoiding the risk of asymmetric usage of ground truths. While performing the prediction, the application of lesion detection and segmentation might have been employed to improve the interpretability of the model, which would have been beneficial to clinical practitioners.

ProCDet, a PCa detection model, was proposed in [14], and this model was comprised of three modules. Initially, the registration of multiple sequences of MR images was done in order to determine a spatial link among the diverse sequences of MR images. Then, using the prostate segmentation networks that was created using the attention mechanism, it was possible to map the PCa and eliminate the interferences of background data from the segmentation. At last, to detect the precise site of PCa, based on Focal Tversky Loss, a 3D PCa lesion segmentation network was implemented to the data. Furthermore, the accuracy of PCa detection was improved through the application of a self-supervised learning strategy. The model's shortcomings include that the labelling information in the training data was not very good and that it required a significant amount of processing effort.

In general, the deep learning CNN performs similarly on images taken with and without an endorectal coil, according to the research. In [15], using a holistically nested edge detector and deep CNN was proposed to classify and detect PCa. The HED-based architecture was refined in order to provide probability maps that were medically relevant. The use of deep learning systems, in particular, has a disadvantage that is intrinsic to all machine learning systems, as effective methods for interpreting neural networks have not yet been created. When this model failed to identify an "obvious" lesion with a very high probability of being PCa, it was considered a significant flaw in the system.

## 3. PROPOSED REGNET MODEL

The PCa is classified in this research based on the T2w-MR images, which were obtained from the prostate dataset. The proposed RegNetY-320 model is a pretrained deep transfer learning model based on deep learning, which was used for the classification of PCa. A subset of MR images from 845 patient records with a unique "UCLA" score of the ROI was used for multi class classification from the proposed dataset. The RegNetY-320 transfer learning model was optimized using the Adam, AdaMax, SGD, RMSprop, Ftrl, and Nadam optimizers in order to classify the information in the data. These optimizers were used to optimize the models with respect to the learning rate in order to execute the classification task. Finally, on the basis of the findings, the performances of the various proposed models were evaluated in order to determine their validity.

RegNetnetwork model design spaces that configure network populations. In [16], the RegNet model was introduced, and it was used to investigate the structure aspect of network design, leading to the discovery of a low-dimension design spaces comprising of simple, regular network, which is referred to as RegNet. In the beginning, the researchers established a design space called AnyNet, which consists of three segments: a stem, body, and head. The typical residual bottlenecks block,

ISSN 1819-6608
ARPN Journal of Engineering and Applied Sciences



referred to as a X block, and the AnyNet design spaces constructed on top of it, referred to as AnyNetX, are used in the majority of trials. Following the development of several rules and the search for the efficient models, the last created model was designated as RegNetX. RegNetY was discovered by assessing the RegNetX with Squeeze and Excitation (SE) operations and comparing the results.
The RegNetwas based on the idea of finding simple models that were simple to comprehend, build upon, and generalized as a starting point. It is included in the RegNet model a novel network design model that integrates the benefits of manual designing with the advantages of Neural Architecture Search (NAS). NAS overcomes the limits of manual network design and assists in the discovery of an appropriate model within a fixed search area of feasible networks. To the contrary, this RegNet model made use of semi-automated techniques and concentrated on designing design spaces, which aid in the parametrization of the population of networks, as opposed to human design. A design space design is the term used to describe this procedure. Design space can be thought of as a broad, potentially endless population of model structures [17].

As illustrated in Figure-1, all the networks consist of a stem (stride-2 3x3 conv with $w_0$ = 32 channels of output), subsequently by the body of network, which performed the majority of the computations, and finally the head (average pooling subsequent to a FC layer) that predict $n$ output classes. Figure-1 shows the structure of network. With $r_i$ decreasing in value as the network grows in size, the network body was comprised of stages that operates at decreasing resolutions. Every stage was comprised of a series of similar blocks, with the exception of the first block, which makes use of stride-two convolution. Despite the fact that the overall structure was simple, the overall conceivable configurations of network was large.

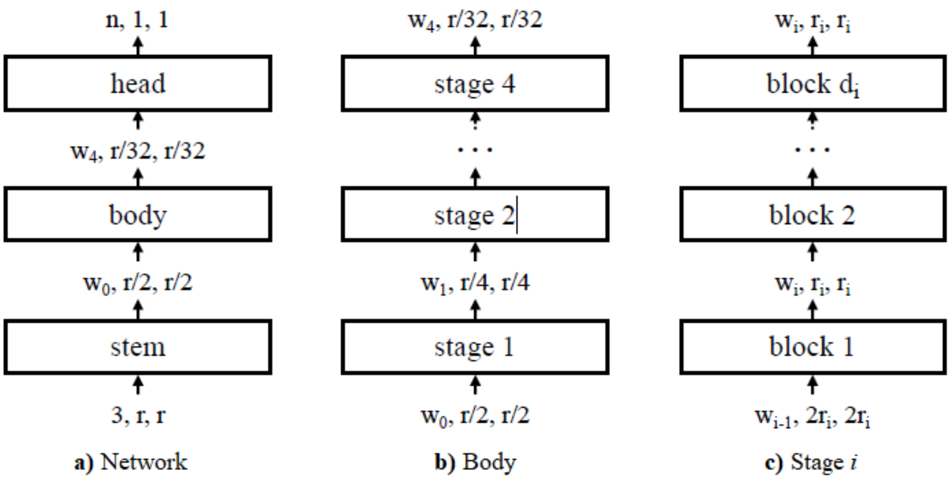


**Figure-1.** Common structure of networks for design space models [18].

As illustrated in Figure-2, every stage consists of a stride $s$ = 2 block that reduces $r$ by half and raises $w$, followed by a series of stride $s$ = 1 blocks with constant $r$ and $w$. Residual bottlenecks along with group convolutions form the basis of the $Y$ block. In every block, there is a 1x1 convolution layer, a 3x3 group convolution layer, and a final 1x1 convolution layer. The bottleneck ratio b of the 1x1 conv layer can be used to modify the value of $w$; however, $b$ is set to 1. BatchNorm and ReLU are applied after every conv layer.

ARPN Journal of Engineering and Applied Sciences



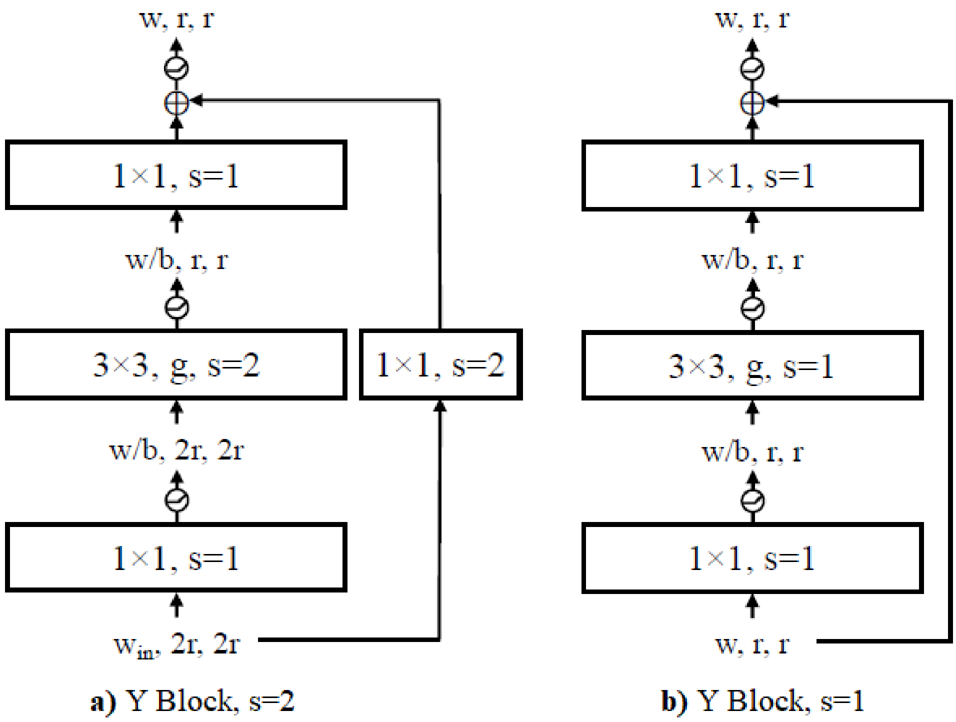


**Figure-2.** RegNetY blocks [18].

The stage widths and depths that make up the RegNet design space cores were resolved by the quantized linear functions. This RegNet design space was created in a low-epoch, low-computational environment, utilizing a type of single network block on the ImageNet dataset. During each phase of the design, the input was a preliminary design space and the output was the refined design space, with all the design steps aiming to find design principles that result in populations of models that are either simpler or better performing than before. The error empirical distribution function (EDF) is the key instrument for evaluating the quality of design space designs. During the construction of RegNet, a relatively unrestricted design space known as AnyNet was employed, in which the depths and widths may change freely between stages. The EDF is the most important instrument for evaluating the quality of a design space. EDF of $n$ models with errors $e_i$ is given by:

$$F(e) = \frac{1}{n}\sum_{i=1}^{n} 1[e_i < e] \quad (1)$$

where $F(e)$ is the proportion of models with errors smaller than $e$ and $n$ is the number of models with errors.

The Y block is similar to the regular residual bottleneck block, except it contains group convolutional layers instead of individual convolution layers. In addition, it makes use of the SE layer. The bottleneck ratio $b$ was determined to be one (effectively no bottleneck). Thus, a RegNetY model may be given completely with only five parameters: $d$, $w_0$, $w_a$, $w_m$, and $g$.

A design space of convolutional network with basic, normal models, with parameters: starting width $w_0 > 0$, depth $d$, and slope $w_a > 0$, and it creates a diverse block width $u_j$ for every block $j < d$. The most important requirement for RegNet model types was that the block widths are parameterized linearly (the design spaces only contain models with the linear structures):

$$u_j = w_0 + w_a \cdot j \text{ for } 0 \leq j < d \quad (2)$$

It was necessary to incorporate an additional parameter $w_m > 0$ in order to quantize $u_j$. This parameter regulates quantization in the following ways. Initially, given $u_j$ from the equation 2, the following computation was done to $s_j$ for all the blocks$j$ to ensure as follows:

$$u_j = w_0 \cdot w_m^{s_j} \quad (3)$$

In order to quantize $u_j$, the$s_j$was simply round (which was indicated by $[s_j]$) and calculate quantized per-block width $w_j$ using the following procedure:

$$w_j = w_0 \cdot w_m^{[s_j]} \quad (4)$$

Additional constraints apply in the RegNetX: where the bottleneck ratio $b$ is set to 1, $12 \leq d \leq 28$, and $w_m \geq 2$ (width multiplier). There is only one modification for RegNetY, and that is the addition of SE blocks. The architecture of RegNetY-320 is composed of the following layers: 1x1 Convolution, Convolution, Batch Normalization, Dense Connections, Grouped Convolution, Global Average Pooling, ReLU, and SE Block. The RegNetY-320 model has a parameter size of 145 million and a flop count of 41 billion [19].

VOL. 18, NO. 2, JANUARY 2023 ISSN 1819-6608
ARPN Journal of Engineering and Applied Sciences



The proposed model RegNetY-320 was trained using different optimizers like Adam, AdaMax, SGD, RMSprop, Ftrl, and Nadam techniques. Based on these six optimizers six models were developed to classify the PCa.

- RegNetY-320 Model-01 was modified with Adam (Adaptive Moment Estimation) optimizer with 0.001 learning rate.
- RegNetY-320 Model-02 was modified with SDG (Stochastic Gradient Descent) optimizer with 0.001 learning rate.
- RegNetY-320 Model-03 was modified with RMSprop (Root Mean Squared propagation) optimizer with 0.00001 learning rate.
- RegNetY-320 Model-04 was modified with Ftrl (Follow the Regularized Leader) optimizer with 0.001 learning rate.
- RegNetY-320 Model-05 was modified with AdaMax(Extension of Adam) optimizer with 0.00001 learning rate.
- RegNetY-320 Model-06 was modified with Nadam (Nesterov-accelerated Adaptive Moment Estimation) optimizer with 0.001 learning rate.

## 4. EXPERIMENTAL ANALYSIS

The Python 3.7.12 programming language tool was used for the design and development of proposed models. The tests are carried out on Google Colab Pro, a cloud-based collaboration platform. The data was collected for the TCIA website, which was provided by the University of California, Los Angeles (UCLA), and was used in this research for the evaluation.

### A. Dataset Description

An image dataset with a total size of 77.6 GB is contained in this Prostate-MRI-US-Biopsy dataset, which comprises US and MR images of 1151 individuals as well as 61,119 DICOM images. The mpMRI sequences T2W, DW, and DCE were used to establish MRI targets, which were then scored on a Likert-like scale that was closely comparable to the PIRADS version 2 scale, which was utilized to grade the MRI targets. MRI was used to delineate the ROI outlines because it was the only sequence included in this data collection that used t2-weighted imaging. The MRI was performed on a Verio, Skyra, or 3 Tesla Trio scanner, depending on which manufacturer was used to perform the scan (Siemens, Erlangen, Germany). In all patients, a transabdominal phased array was used, with an endorectal coil being used in a subset of cases to complete the treatment. Pulse sequences for 3D T2:SPC imaging account for the vast majority of all sequences, with the most common being TR/TE values of 2200/203, Matrix/FOV values of 256x205/14x14 cm and 1.5mm slice spacing, respectively [20].The dataset can be download from this link Prostate MRI and Ultrasound With Pathology and Coordinates of Tracked Biopsy (Prostate-MRI-US-Biopsy).

This dataset was made available to the public through a data sharing portal. In order to perform Multi Class Classification, a subset of T2W MR Images from 845 patient records that had a unique "UCLA" score of the ROI was selected from the dataset and used for evaluation. In order to conduct performance analysis, the data set was separated into two parts: 70% for training and 30% for testing. In contrast to a numerical scale, a Likert-like score was a visual analogue scale on which scores of 1-5 indicated the likelihood of PCa based on the total number of interpretations of the prostate MRI by a radiologist, rather than a numerical scale. Scores of 1 and 2 suggest a low suspicion of cancer, 3 indicates an equivocal suspicion, and 4 or 5 indicate a high suspicion of cancer. Here, the value zero represents the normal/healthy state of the image.

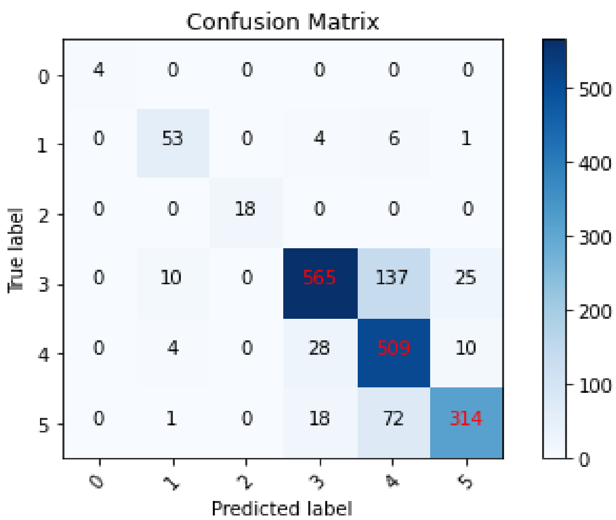


**Figure-3.** Confusion matrix for RegNet-model-01.

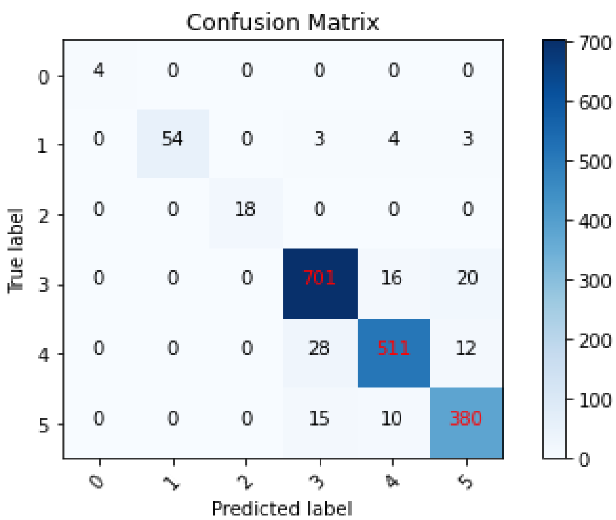


**Figure-4.** Confusion matrix for RegNet-model-02.

VOL. 18, NO. 2, JANUARY 2023 ISSN 1819-6608
ARPN Journal of Engineering and Applied Sciences

www.arpnjournals.com

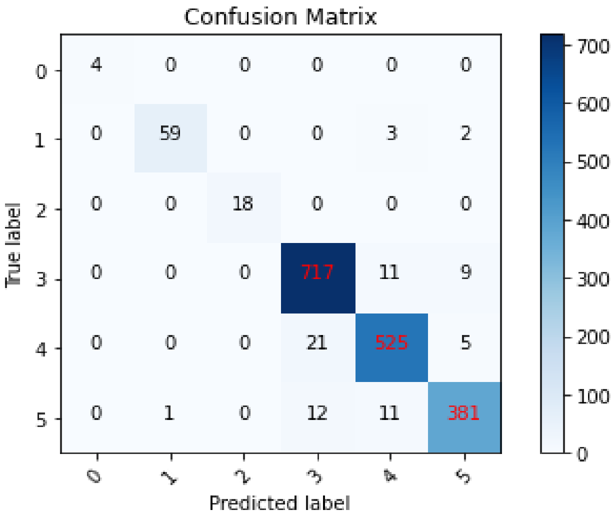


**Figure-5.** Confusion matrix for RegNet-model-03.

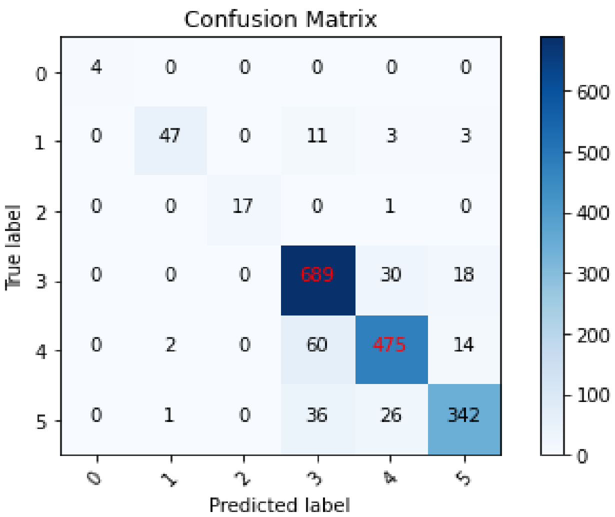


**Figure-6.** Confusion matrix for RegNet-model-04.

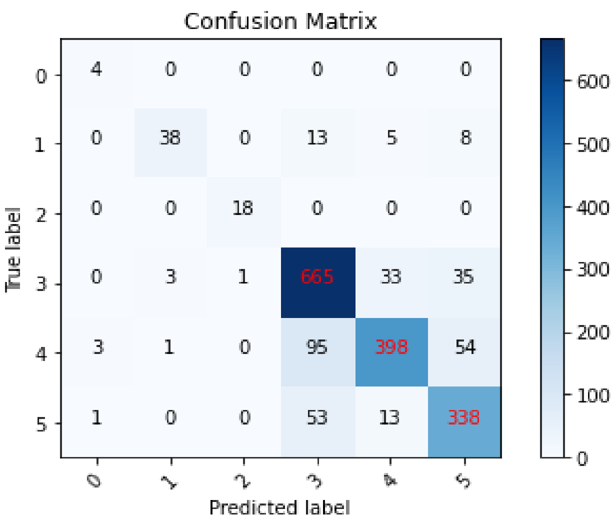


**Figure-7.** Confusion matrix for RegNet-model-05.

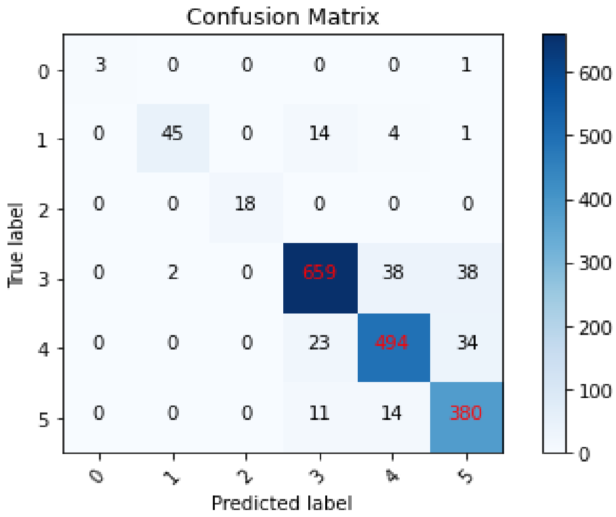


**Figure-8.** Confusion matrix for RegNet-model-06.

Figures 3 to 8 represents the confusion matrix computations of the proposed RegNetY-320 models. The models optimized using different optimizers as discussed earlier were computed individually for proper validation. Based on these confusion matrix computations, the performances of the proposed models were evaluated using the following performance metrics.

### B. Performance Metrics

With T2w-MR images, the main purpose of the research is to classify and detect PCa in patients. This can be used to determine whether or not the patient has PCa. The accuracy, sensitivity, precision, specificity, and F1-score were used to calculate the findings of this analysis. When computing the outcome of this model, the true positive, false positive, true negative, and false negative were all thoroughly examined and analyzed.

**TP:** This variable represents the total number of properly predicted outcomes in positive cases.

**FP:** This variable reflects the total number of incorrect predictions acquired in positive cases.

**TN:** This variable reflects the total number of properly predicted outcomes in negative cases.

**FN:** This value represents the total number of predictions in negative cases.

$$Accuracy = \frac{TP+TN}{TP+TN+FP+FN} \tag{5}$$

$$Precision = \frac{TP}{TP+FP} \tag{6}$$

$$Sensitivity = \frac{TP}{TP+FN} \tag{7}$$

$$Specificity = \frac{TN}{TN+FP} \tag{8}$$

$$F1\ Score = 2 \times \frac{Precision \times Recall}{Precision+Recall} \tag{9}$$

The classification performances of the proposed models are measured using the metrics as given in equations (5) to (9). Each of these metrics is measured and plays an important role in evaluating the classification performances of the proposed model.

**Table-2.** Comparison of accuracy performance.

| Class | Adam | SGD | RMSprop | Ftrl | Adamax | Nadam |
|---|---|---|---|---|---|---|
| 0 | 0.822 | 0.937 | 0.957 | 0.884 | 0.941 | 0.898 |
| 1 | 0.822 | 0.937 | 0.957 | 0.884 | 0.941 | 0.898 |
| 2 | 0.822 | 0.937 | 0.957 | 0.884 | 0.941 | 0.898 |
| 3 | 0.822 | 0.937 | 0.957 | 0.884 | 0.941 | 0.898 |
| 4 | 0.822 | 0.937 | 0.957 | 0.884 | 0.941 | 0.898 |
| 5 | 0.822 | 0.937 | 0.957 | 0.884 | 0.941 | 0.898 |

Table-2 represents the accuracy performances of the proposed RegNetY-320 models ranging from RegNetY-320_Model-01 to RegNetY-320_Model-06. All the models obtained a constant accuracy for each class of the dataset. The model-03 optimized using RMSprop optimizer with 0.0001 learning rate obtained a highest accuracy of 95.70%, following the model-05 optimized using Adamax optimizer with 0.0001 learning rate obtained 94.10%. The least accuracy was obtained from model-01 optimized using Adam optimizer with 0.001 learning rate. There is a huge marginal difference of 1.6 to 13.5% from the performance compared model-03 with other models. Figure-9 represents the accuracy comparison of proposed models.

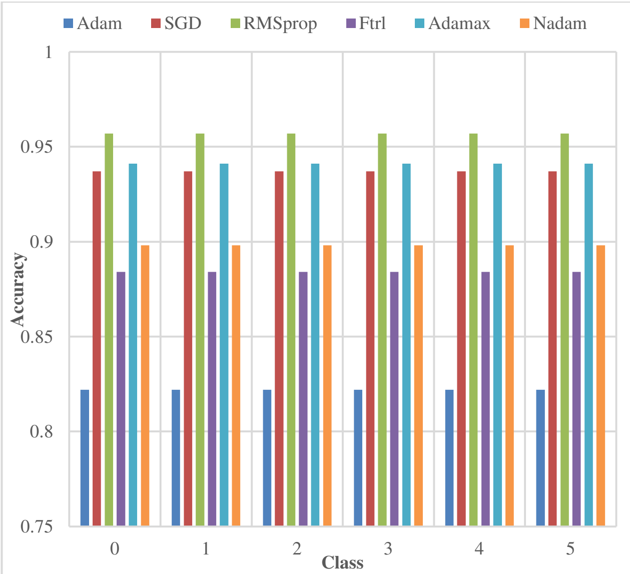


**Figure-9.** Graphical plot for accuracy comparison.

**Table-3.** Comparison of precision performance.

| Class | Adam | SGD | RMSprop | Ftrl | Adamax | Nadam |
|---|---|---|---|---|---|---|
| 0 | 1 | 1 | 1 | 1 | 1 | 0.75 |
| 1 | 0.828 | 0.843 | 0.921 | 0.734 | 0.875 | 0.703 |
| 2 | 1 | 1 | 1 | 0.944 | 1 | 1 |
| 3 | 0.766 | 0.951 | 0.972 | 0.934 | 0.964 | 0.894 |
| 4 | 0.923 | 0.927 | 0.952 | 0.862 | 0.940 | 0.896 |
| 5 | 0.775 | 0.938 | 0.940 | 0.844 | 0.908 | 0.938 |

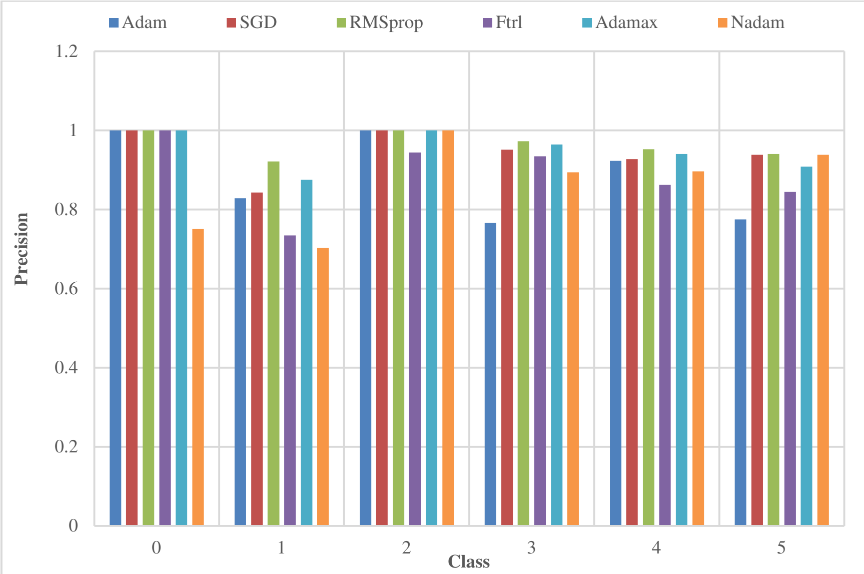


**Figure-10.** Graphical plot for precision comparison.

The precision evaluation of the proposed RegNetY-320 models were tabulated in Table-3. There were variations in the performances of all the models for each class of the dataset. Constantly, the models-01 to 05 obtained same precision for class 0 and similar constant in class 2. Here, the model-03 optimized using RMSprop optimizer with 0.0001 learning rate obtained a better precision compared to other models. The least precision was obtained from model-01 optimized using Adam optimizer with 0.001 learning rate. Figure-10 represents the precision comparison of proposed models.

**Table-4.** Comparison of sensitivity performance.

| Class | Adam | SGD | RMSprop | Ftrl | Adamax | Nadam |
|---|---|---|---|---|---|---|
| 0 | 1 | 1 | 1 | 1 | 1 | 1 |
| 1 | 0.779 | 1 | 0.983 | 0.94 | 1 | 0.957 |
| 2 | 1 | 1 | 1 | 1 | 1 | 1 |
| 3 | 0.918 | 0.938 | 0.956 | 0.865 | 0.939 | 0.932 |
| 4 | 0.703 | 0.944 | 0.954 | 0.887 | 0.923 | 0.898 |
| 5 | 0.897 | 0.915 | 0.959 | 0.907 | 0.960 | 0.837 |

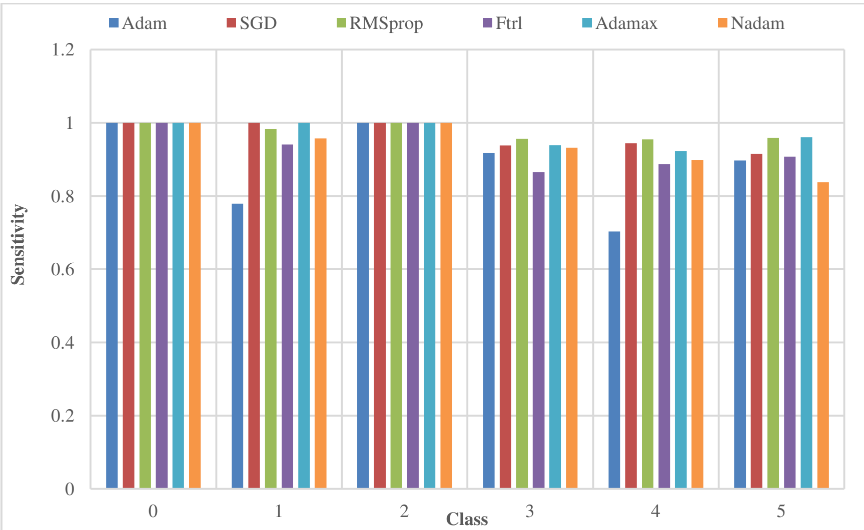


**Figure-11.** Graphical plot for sensitivity comparison.

ARPN Journal of Engineering and Applied Sciences



Table-4 represents the sensitivity performances of the proposed RegNetY-320 models. There were variations in the performances of all the models for each class of the dataset. Constantly, the models-01 to 06 obtained same sensitivity for class 0 and similarly constant in class 2. Here, the model-03 optimized using RMSprop optimizer with 0.0001 learning rate obtained a better precision compared to other models. The least sensitivity was obtained from model-01 optimized using Adam optimizer with 0.001 learning rate. Figure-11 represents the sensitivity comparison of proposed models.

**Table-5.** Comparison of specificity performance.

| Class | Adam | SGD | RMSprop | Ftrl | Adamax | Nadam |
|---|---|---|---|---|---|---|
| 0 | 1 | 1 | 1 | 1 | 1 | 0.999 |
| 1 | 0.992 | 0.993 | 0.996 | 0.988 | 0.995 | 0.987 |
| 2 | 1 | 1 | 1 | 0.999 | 1 | 1 |
| 3 | 0.839 | 0.964 | 0.980 | 0.948 | 0.973 | 0.923 |
| 4 | 0.957 | 0.966 | 0.978 | 0.935 | 0.972 | 0.950 |
| 5 | 0.926 | 0.980 | 0.982 | 0.951 | 0.972 | 0.979 |

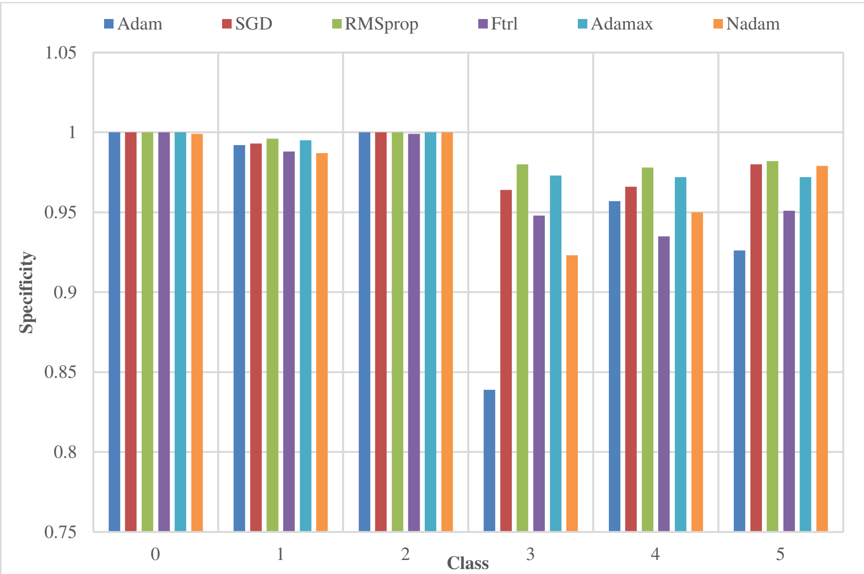


**Figure-12.** Graphical plot for specificity comparison.

The specificity evaluation of the proposed RegNetY-320 models were tabulated in Table-5. There were variations in the performances of all the models for each class of the dataset. Almost, all the models-01 to 06 obtained same specificity score for class 0 and in class 2. Here, the model-03 optimized using RMSprop optimizer with 0.0001 learning rate obtained a better specificity compared to other models. The least specificity was obtained from model-01 optimized using Adam optimizer with 0.001 learning rate. Figure-12 represents the specificity comparison of proposed models.

**Table-6.** Comparison of F1-score performance.

| Class | Adam | SGD | RMSprop | Ftrl | Adamax | Nadam |
|---|---|---|---|---|---|---|
| 0 | 1 | 1 | 1 | 1 | 1 | 0.857 |
| 1 | 0.803 | 0.915 | 0.951 | 0.824 | 0.933 | 0.810 |
| 2 | 1 | 1 | 1 | 0.971 | 1 | 1 |
| 3 | 0.835 | 0.944 | 0.964 | 0.898 | 0.951 | 0.912 |
| 4 | 0.798 | 0.935 | 0.953 | 0.874 | 0.931 | 0.897 |
| 5 | 0.831 | 0.926 | 0.950 | 0.874 | 0.934 | 0.884 |

Table-6 represents the F1-Score performances of the proposed RegNetY-320 models. There were variations in the performances of all the models for each class of the dataset. Constantly, the models-01 to 05 obtained same F1-scores for class 0 and similarly constant in class 2. Here, the model-03 optimized using RMSprop optimizer with 0.0001 learning rate obtained a better specificity compared to other models. The least specificity was obtained from model-01 optimized using Adam optimizer with 0.001 learning rate. Figure-13 represents the F1-Score comparison of proposed models.

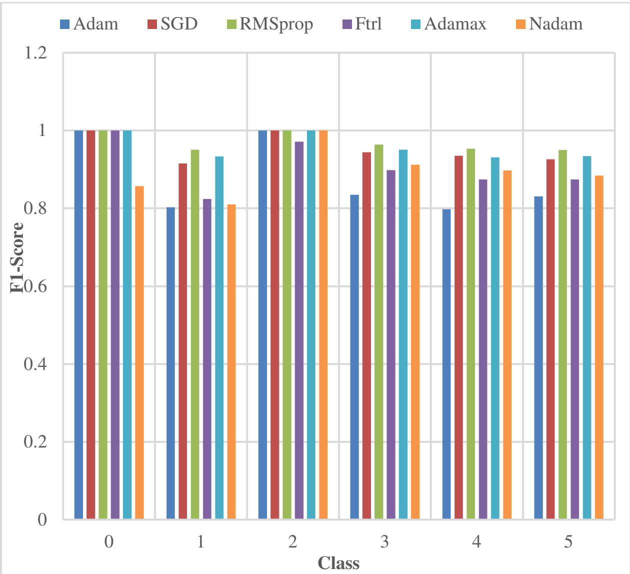


**Figure-13.** Graphical plot for F1-score comparison.

According to the obtained performances, the proposed RegNetY-320_Model-03 optimized using RMSprop optimizer has obtained better performances compared to the other proposed RegNetY-320 models. This RegNetY-320_Model-03 obtained 95.70% accuracy, which is the best accuracy rate obtained in this research. The least performances were obtained from the RegNetY-320_Model-01 with 82.20% accuracy as well as low performances in other parameters too.

## 5. CONCLUSIONS

In this research, a deep learning approach was proposed to classify the PCa with the help of T2w MRI dataset images. The proposed RegNetY-320 architecture was trained and tested on different optimizers with different learning rates as discussed above and these models were termed as Model-01 to Model-05. The Prostate-MRI-US-Biopsy dataset was used for the evaluation of the proposed models, which contains both US and MR Images of 1151 patients, and 61,119 DICOM Images. From the dataset, only the subset T2w MR Images of 845 patient records with unique "UCLA" score of the ROI was used for Multi Class Classification. For performance analysis, the data set was split into 70% for training and 30% for testing. Although, a series of different optimizers were used to optimize the proposed model with different learning rates, the model optimized with RMSprop optimizer performed well with obtaining best performances compared to the other proposed models. According to the obtained performances, the proposed RegNetY-320_Model-03 optimized using RMSprop optimizer has obtained better performances compared to the other proposed RegNetY-320 models. The RegNetY-320_Model-03 obtained 95.70% accuracy, which is the best accuracy rate obtained in this research. The least performances were obtained from the RegNetY-320_Model-01 with 82.20% accuracy as well as low performances in other parameters too. In future, the proposed model can be used to perform the prostate classification on various MRI sequences other than T2w like DWI, ADC for additional enhancement.

## REFERENCES

[1] Retta C Sihotang *et al.* 2022. The accuracy of machine learning models using ultrasound images in prostate cancer diagnosis: A systematic review. medRxiv, [Online].

[2] Henrik J. Michaely *et al.* 2022. Current Value of Biparametric Prostate MRI with Machine-Learning or Deep-Learning in the Detection, Grading, and Characterization of Prostate Cancer: A Systematic Review. Diagnostics, 12, 799, 2022.

[3] Niranjan J Sathianathen *et al.* 2019. Accuracy of the magnetic resonance imaging pathway in the detection of prostate cancer: a systematic review and meta-analysis. Prostate cancer and prostatic diseases. 22(1): 39-48.

[4] Huanye Li *et al.* 2022. Machine Learning in Prostate MRI for Prostate Cancer: Current Status and Future Opportunities. Diagnostics. 12, 289.

[5] Shaun A Wahab and SadhnaVerma. 2016. Review of prostate imaging reporting and data system version 2. Future Oncology. 12(21): 2479-2494.

[6] Ahmad Chaddad *et al.* 2021. Magnetic resonance imaging based radiomic models of prostate cancer: A narrative review. Cancers. 13, 552.

[7] Amita Shukla-Dave and HedvigHricak. 2014. Role of MRI in prostate cancer detection. NMR in Biomedicine. 27: 16-24.

[8] Eleni Chiou *et al.* 2018. Prostate cancer classification on VERDICT DW-MRI using convolutional neural networks. International Workshop on Machine Learning in Medical Imaging. 11046.

[9] Yohannes K. Tsehay *et al*. 2017. Convolutional neural network based deep-learning architecture for prostate cancer detection on multiparametric magnetic resonance images. Medical imaging 2017: Computer-aided diagnosis. 10134.

[10] Xin Yang *et al*. 2017. Co-trained convolutional neural networks for automated detection of prostate cancer in multi-parametric MRI. Medical image analysis. 42: 212-227.

[11] Ruiming Cao *et al*. 2019. Joint prostate cancer detection and Gleason score prediction in mp-MRI via FocalNet. IEEE transactions on medical imaging, 38(11): 2496-2506.

[12] Yulian Zhu *et al*. 2017. MRI-based prostate cancer detection with high-level representation and hierarchical classification. Medical physics. 44(3):1028-1039.

[13] Lizhi Shao *et al*. 2021. Patient-Level Prediction of Multi-Classification Task at Prostate MRI Based on End-to-End Framework Learning from Diagnostic Logic of Radiologists. IEEE Transactions on Biomedical Engineering. 68(12): 3690-3700.

[14] Yuejing Qian, Zengyou Zhang and Bo Wang. 2021. ProCDet: A New Method for Prostate Cancer Detection Based on MR Images. IEEE Access, 9:143495-143505.

[15] Yohan Sumathipala *et al*. 2018. Prostate cancer detection from multi-institution multiparametric MRIs using deep convolutional neural networks," Journal of medical imaging, 5(4), 044507, 2018.

[16] IlijaRadosavovic *et al*. 2020. Designing network design spaces. Proceedings of the IEEE/CVF Conference on Computer Vision and Pattern Recognition (CVPR), pp. 10428-10436, 2020.

[17] Wentao Zhao *et al*. 2021. Compare the performance of the models in art classification. Plos one, 16(3): e0248414, 2021.

[18] Piotr Dollar, Mannat Singh, and Ross Girshick, "Fast and accurate model scaling. Proceedings of the IEEE/CVF Conference on Computer Vision and Pattern Recognition, pp. 924-932, 2021.

[19] Lijun Wang *et al*. 2022. Evaluation of a deep learning model for multi-spectral remote sensing of land use and crop classification. The Crop Journal.

[20] Natarajan S *et al*. 2020. Prostate MRI and Ultrasound with Pathology and Coordinates of Tracked Biopsy (Prostate-MRI-US-Biopsy) Dataset.